ELSEVIER

Journal of Fluids and Structures 25 (2009) 777–793

JOURNAL OF FLUIDS AND STRUCTURES

www.elsevier.com/locate/jfs

# The effect of submergence on the scattering by the interface between two semi-infinite sheets

T.D. Williams*[,1], R. Porter

*Department of Mathematics, University of Bristol, University Walk, Bristol, BS8 1TW, UK*

Received 25 September 2008; accepted 16 February 2009
Available online 7 April 2009

**Abstract**

This paper considers the reflection and transmission of a flexural-gravity wave within ice sheets floating on water as it propagates through a series of abrupt changes in ice sheet characteristics. The canonical problem involves one such junction at which two semi-infinite ice sheets of different properties are either frozen together or separated by a crack. Unlike most mathematical approaches to problems involving ice sheets, we allow the ice sheets to adopt a variable submergence according to their thickness. The problem is solved using integral equations formulated through the matching of eigenfunction expansions.


*Keywords:* Wave-ice interaction; Sea-ice; Finite draft; Galerkin scheme

## 1. Introduction

In the last decade, a considerable number of papers have been written which aim to determine the scattering properties of a variety of inhomogeneities in ice sheets floating on water. These include features such as leads (open stretches of sea water between two ice sheets) and cracks which form when ice sheets fracture as well as pressure ridges (often forming both 'keels' below and 'sails' above the otherwise constant lower and upper levels of the ice sheets) which form when two ice sheets are compressed by currents and/or wind stress [e.g. Wadhams (1988), who also provides some statistical distributions for such features].

Thus the large polar ice sheets that form across the Arctic and Antarctic seas are embedded with a variety of different structures all of which have an effect on the propagation of hydroelastic waves whose energy originates from the transmission of ocean surface waves into flexural waves at the boundary of the marginal ice zone.

There are good reasons to be interested in the wave propagation across the ice sheets. First, wave action is one of the factors assisting the breakup of ice (in turn accelerating the melting of sea ice) and thus it is useful to be able to approximate how far waves can propagate through an ice field. Secondly, it may be possible to use inverse scattering ideas along with a statistical knowledge of the distribution of inhomogeneities to determine the thickness of the ice. Remote sensing of the wave propagation across ice sheets can be done efficiently and continuously using satellite

*Corresponding author. Tel.: +44 117 331 8224; fax: +44 115 928 7999.
*E-mail address:* timothy.williams@bristol.ac.uk (T.D. Williams).
[1]Supported by a post-doctoral fellowship from the New Zealand Foundation of Research, Science and Technology (FRST) and by the University of Bristol.

0889-9746/$ - see front matter © 2009 Elsevier Ltd. All rights reserved.
doi:10.1016/j.jfluidstructs.2009.02.001

interrogated wave buoys and thus an inverse scattering approach for determinating ice thickness is an extremely attractive prospect. In contrast, current methods which rely on taking manual measurements of ice thickness are slow and costly. The determination of ice thickness is an area of key importance given the current concern of the retreat of summer sea ice in the Arctic seas.

This second reason was the main motivation for undertaking the present paper. Our results are currently being used in collaborative work between the first author and V.A. Squire (University of Otago), in the calculation of the scattering by ice fields containing a large number of leads. In trials to date, the scattering thus obtained was fitted with a simpler curve based on average scattering and a thickness estimate produced. The results of doing this seem promising.

The importance of accurately and efficiently determining the reflection and transmission properties from each feature is therefore of some importance. These fundamental problems, as described at the beginning of the introduction must come under scrutiny. In these linear hydroelastic problems, it is has been common practice for researchers to assume that the ice sheet 'floats' on top of the water so that the underside of the ice sheet occupies the same horizontal plane as the mean open water level, irrespective of changes in ice thickness. For two identical ice sheets separated by a narrow crack (Squire and Dixon, 2000; Evans and Porter, 2003) this is not an issue. But when considering scattering by changes in ice thickness (for example, through a pressure ridge) it is not physically realistic to ignore the submergence of the ice sheet and assume the extra mass of ice simply sits above the waterline. Largely because of the mathematical difficulties of incorporating changes of submergence of the ice sheet, but also because of the seemingly small drafts of irregularities in comparison to the wavelengths of ice-coupled waves (which for 1-m-thick ice are commonly between 50 and 600 m) many researchers have continued to calculate scattering without including submergence [e.g. Williams and Squire (2004, 2007) and Kohout et al. (2007)]. This is also routinely done when modelling ice floes in open water [e.g. Meylan and Squire (1994) and Wang et al. (2007)]. Indeed, Williams and Squire (2008a) show that when considering an iceberg embedded into an ice sheet or an ice floe in open water, results for an individual feature obtained from neglecting submergence are qualitatively very similar to those obtained when the correct draft is included. However, small differences can add up, especially when large numbers of irregularities are considered, and so it is valuable to have an accurate and efficient method of dealing with submergence [also considered in the work of Wu et al. (1995), Porter and Porter (2004) and Bennetts et al. (2007)].

In the current paper, we approach the problem of the transmission of oblique waves through a junction between two semi-infinite ice sheets of (generally) different but uniform thickness (see Fig. 1). Each sheet individually obeys Archimedes' law; consequently there exists a step in the lower profile of the ice sheet along the line of the junction. This is a problem which is not amenable to the mild-slope method of Porter and Porter (2004); it could also be treated by adapting the methods of Wu et al. (1995) and Bennetts et al. (2007), although our method has the advantage that it takes into account the singularity in the velocity potential at the lower corner of the step which produces extremely good convergence. This single step problem is the canonical problem to consider when the horizontal distance over which the thickness changes is much less than the shortest wavelength in the spectrum (typically about 50 m), as in the two edges of a lead.

In the problem under consideration here, we allow the junction between the two ice sheets of different thickness to be either frozen or to contain a narrow crack. The method of solution involves expanding either side of the junction, under each semi-infinite ice sheet, in a set of non-orthogonal eigenfunctions. We use a matching procedure at the junction which takes into account continuity of fluid velocity and pressure, and applies no normal flow on the vertical face of the thicker ice sheet in addition to the application of free bending and shearing conditions on the edge of each ice sheet. The problem is formulated as an integral equation for an unknown horizontal fluid velocity, $u(z)$, in the vertical matching interval below the ice sheets in a manner similar to that used by Porter (1995) for surface wave scattering by vertical steps in the sea bed. It is shown that the key quantities are readily determined as inner products of $u(z)$ with the forcing functions in the integral equation, which is itself solved by using a Galerkin scheme which takes into account corner singularities in the velocity potential. This Galerkin-based formulation has not been used previously in the area of ice sheets. However, it is a completely general method that has seen widespread use in other linear field theories such as water waves, acoustics and electromagnetics [see, for example, Porter (1995) and Linton and McIver (2001)], and it is characterised by efficient and accurate numerical solutions.

In Section 2, the governing equations are stated and the integral equation is formulated by application of various conditions. The Galerkin approximation is implemented in Section 3, giving rise to the systems of equations that are solved numerically. In Section 4 we show how reflection and transmission coefficients can be obtained when there are multiple junctions by applying the wide-spacing approximation. In the short Section 5, we briefly discuss the system that arises and the equations that need to be solved when considering the possibility of edge waves travelling either side of a crack. For ice sheets of the same thickness either side of the crack, Evans and Porter (2003) showed that edge waves existed very close to the cut-off frequency. These edge waves are exponentially decaying in the direction perpendicular to the crack, but travel along the crack with a wavenumber close to the wavenumber for propagation in the absence of

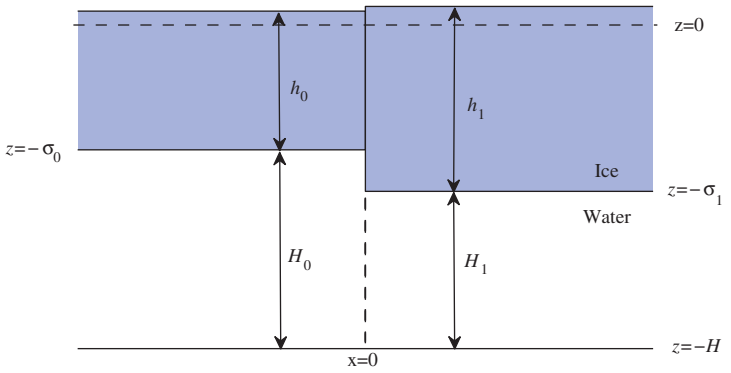


Fig. 1. Geometry of the problem being considered. The coordinate system used is chosen so that $z=0$ corresponds to the position of the free air–water surface if the ice were to melt, and so that $H$ would be the depth if this happened. The figure shows the thicknesses and submergences of the two ice sheets—respectively, these are $h_j$ and $\sigma_j$ (for $j=0,1$, where $j=0$ corresponds to the left hand side, and $j=1$ to the right hand side). The water depths on each side of the interface between the two ice sheets (which is located at $x=0$; $x$ increases to the right) are $H_0$ and $H_1$. In the current paper we study the scattering of plane waves which may be obliquely incident from either region. The angle that the waves make to the $x$ axis is $\theta_j$ ($j=0,1$)—this depends on the region they originate from as the waves will be diffracted as they pass from one to the other.

the crack. In Evans and Porter (2003), the edge wave was shown to be symmetric about the crack. Because of the difference in ice sheet thickness, the symmetry is destroyed. It is shown that edge waves exist only for very small perturbations from equal thickness. The results are described in Section 6 and finally the paper is summarised in Section 7.

## 2. Governing equations and formulation of integral equations

The geometry of the problem being considered is shown in Fig. 1. Cartesian coordinates $(x,y,z)$ are chosen with $z$ pointing vertically upwards and the $z=0$ aligned with the position of the undisturbed free surface of a fluid in the absence of ice. The fluid is assumed to be of constant density $\rho$, and to have a flat bottom located at $z=-H$. Two different ice sheets each of uniform density and thickness now cover the fluid, and meet one another along the plane $x=0$. In $x<0$, the ice sheet is of density $\rho_0$, flexural rigidity $D_0$ and is of thickness $h_0$. In $x>0$, the corresponding parameters are $\rho_1$, $D_1$ and $h_1$. The flexural rigidity is defined in terms of a Young's modulus $E_j$, Poisson ratio $v_j$, as $D_j=\frac{1}{12}E_jh_j^3/(1-v_j^2)$, $j=0,1$. Archimedes' Law implies that the submergence either side of $x=0$ is related to the thickness via $\sigma_j=h_j(\rho_j/\rho)$, making the water depth $H_j=H-\sigma_j$. At the interface between the two ice sheets, the edges may be either frozen together or free. The physical and mathematical conditions that arise from either case are discussed later.

Time harmonic motion of angular frequency $\omega$ is assumed. We choose $h_1>h_0$, so that the thicker ice sheet occupies the region $x>0$, but in order to retain generality we will allow waves to be obliquely incident from both negative and positive infinity. Because of the uniformity in the $y$-direction (in the direction of the crack), we may take out a constant phase factor, $\alpha_y$, which will eventually be related to the wavenumber and angle of propagating waves in $x<0$ and $x>0$.

Before continuing, it makes sense to nondimensionalise variables in the problem. We begin by defining a characteristic lengthscale $L=(D_1/(\rho\omega^2))^{1/5}$, and some non-dimensional variables and parameters $(\bar{x},\bar{y},\bar{z})=(x,y,z)/L$, $\bar{t}=\omega t$, $\overline{H}=H/L$, $\bar{\sigma}_j=(\rho_jh_j)/(\rho L)$, $\overline{H}_j=H_j/L$, $\overline{D}_j=D_j/D_1$ ($j=0,1$), $\overline{\alpha}_y=\alpha_yL$, and $\kappa=\omega^2L/g$. Here, $\kappa$, the non-dimensional infinite depth open water wavenumber, is the main spectral parameter.

Dropping the overbars now for clarity, we define a velocity potential in terms of the non-dimensional variables and wavenumbers

$$\Phi(x,y,z,t)=\mathscr{R}e[\phi(x,z)\,e^{i(\alpha_y y-t)}], \tag{1}$$

whose gradient determines the velocity of a fluid particle at a given point. The function $\phi$ satisfies the following equations:

$$(\nabla^2-\alpha_y^2)\phi(x,z)=0 \quad \text{in the fluid domain,} \tag{2a}$$

$$(\mathscr{L}_j(\partial_x)\partial_z - 1)\phi(x,-\sigma_j) = 0 \quad \text{for } x \in (-1)^j(-\infty,0) \text{ and } (j=0,1), \tag{2b}$$

$$\partial_x\phi(0^-,z) = 0 \quad \text{for } z \in (-\sigma_1,-\sigma_0), \tag{2c}$$

$$\partial_z\phi(x,-H) = 0, \tag{2d}$$

in addition to edge conditions which we will introduce later. In (2) we have defined the operator

$$\mathscr{L}_j(\partial_x) = D_j(\partial_x^2 - \alpha_y^2)^2 + \kappa^{-1} - \sigma_j.$$

The motion of the ice sheet is governed by a Kirchhoff model (also known as an Euler–Bernoulli thin elastic plate model) and linearised dynamic and kinematic boundary conditions on the underside of the ice sheets are combined to give (2b). For further details on the derivation of Eqs. (2), see the appendix in Williams and Squire (2004).

Now, let $\phi$ be divided into two parts, one on either side of the place $x=0$, by writing

$$\phi(x,z) = \begin{cases} \phi^{(0)}(x,z) & \text{for } (x,z) \in (-\infty,0)\times(-H,-\sigma_0), \\ \phi^{(1)}(-x,z) & \text{for } (x,z) \in (0,\infty)\times(-H,-\sigma_1). \end{cases} \tag{3}$$

Consideration of separation solutions in each semi-infinite domain, under the conditions (2a), (2b) and (2d) allows us to write

$$\phi^{(j)}(x,z) = A_j\,\mathrm{e}^{\mathrm{i}\alpha_j x}\varphi^{(j)}(z,\alpha_j) + \sum_{\alpha\in S_j} R_j(\alpha)\,\mathrm{e}^{-\mathrm{i}\alpha x}\varphi^{(j)}(z,\alpha), \tag{4}$$

where

$$\varphi^{(j)}(z,\alpha) = \frac{\cosh\gamma(\alpha)(z+H)}{\cosh\gamma(\alpha)H_j} \tag{5}$$

are vertical eigenfunctions. The dispersion relations for each side of the domain is defined as $f_j(\alpha) = \Lambda_j(\gamma)\gamma\tanh(\gamma H_j) - 1 = 0$, where $\gamma(\alpha) = \sqrt{\alpha^2+\alpha_y^2}$ and $\Lambda_j(\gamma) \equiv \mathscr{L}_j(\mathrm{i}\alpha) = D_j\gamma^4 + \kappa^{-1} - \sigma_j$. We also define the sets of roots to the dispersion relations as $S_j = \{\alpha \in \mathbb{C} \,|\, f_j(\alpha) = 0 \mid 0 \leqslant \mathrm{Arg}[\alpha] < \pi\}$. Each $S_j$ has a single root $\alpha_j$ such that $\gamma_j = \gamma(\alpha_j)$ is positive real.

Note that in (4), we have allowed waves to be incident from both minus and plus infinity with amplitudes $A_0$ and $A_1$, respectively. The amplitude of waves propagating to minus and plus infinity are $R_0(\alpha_0)$ and $R_1(\alpha_1)$. The wavenumber of propagating waves in $x<0$ and $x>0$ is $\gamma(\alpha_0)$ and $\gamma(\alpha_1)$ and the waves propagate at an angle $\theta_j = \tan^{-1}(\alpha_y/\alpha_j)$ with respect to the plane $y=0$.

The $\varphi^{(j)}$ satisfy the following integral rules for $j=0,1$:

$$\begin{aligned} I^{(j)}(\alpha,\beta) &= -2\alpha B_j^{(2)}(\alpha)\int_{-H}^{-\sigma_j}\varphi^{(j)}(z,\alpha)\varphi^{(j)}(z,\beta)\,dz \\ &= \delta_{\alpha,\beta} + 2\alpha B_j^{(2)}(\alpha)D_j(\alpha^2+\beta^2+2\alpha_y^2)\partial_z\varphi^{(j)}(-\sigma_j,\alpha)\partial_z\varphi^{(j)}(-\sigma_j,\beta) \\ &\equiv \delta_{\alpha,\beta} + 2\alpha B_j^{(1)}(\alpha)D_j(f^{\mp}(\alpha)+f^{\pm}(\beta))\partial_z\varphi^{(j)}(-\sigma_j,\beta), \end{aligned} \tag{6}$$

where $\delta_{\alpha,\beta} = 1$ if $\alpha=\beta$ and zero otherwise, whilst

$$f^{\pm}(\alpha) = \gamma^2(\alpha) \pm (1-\nu)\alpha_y^2 \tag{7}$$

and

$$B_j^{(0)}(\alpha) = \frac{-\gamma^2/\alpha}{H_j(\Lambda_j^2(\gamma)\gamma^2 - 1) + 5D_j\gamma^4 + \kappa^{-1} - \sigma_j}, \tag{8}$$

$$B_j^{(r)}(\alpha) = \Lambda_j^r(\gamma)B_j^{(0)}(\alpha) = B_j^{(2)}(\alpha)(\partial_z\varphi^{(j)}(-\sigma_j,\alpha))^{(2-r)} \quad \text{for } r=1,2, \tag{9}$$

the latter relation having been used with $r=1$ in deriving (6).

Continuity of fluid pressure and velocity implies the matching conditions

$$\left.\begin{aligned} \phi^{(0)}(0,z) &= \phi^{(1)}(0,z) \\ u(z) \equiv \partial_x\phi^{(0)}(0,z) &= -\partial_x\phi^{(1)}(0,z) \end{aligned}\right\} \quad \text{for } z \in (-H,-\sigma_1) \tag{10}$$

(the minus sign against the second derivative is inherited from the definition in (3) and assists in subsequent algebraic manipulations).

Hence

$$\alpha_j A_j \varphi^{(j)}(z,\alpha_j) - \sum_{\alpha\in S_j} \alpha R_j(\alpha)\varphi^{(j)}(z,\alpha) = \begin{cases} 0 & \text{for } z\in(-\sigma_1,-\sigma_j), \\ -\mathrm{i}u(z) & \text{for } z\in(-H,-\sigma_1). \end{cases} \tag{11}$$

For each $j$ ($j=0,1$) we multiply (11) by $-2(-1)^j B_j^{(2)}(\beta)\varphi^{(j)}(z,\beta)$ ($\beta\in S_j$) and integrate with respect to $z$ over $(-H,-\sigma_j)$. Using (6), this gives

$$\begin{aligned} &2(-1)^j B_j^{(2)}(\beta)\mathrm{i}(\mathscr{F}_j u)(\beta) \\ &\quad = A_j\delta_{\beta,\alpha_j} - R_j(\beta) + 2\alpha_j A_1 D_j B_j^{(1)}(\beta)(f^-(\beta)+f^+(\alpha_j))\partial_z\varphi^{(j)}(-\sigma_j,\alpha_j) \\ &\qquad - 2D_j B_j^{(1)}(\beta)\sum_{\alpha\in S_j}\alpha R_j(\alpha)(f^-(\beta)+f^+(\alpha))\partial_z\varphi^{(j)}(-\sigma_j,\alpha) \end{aligned} \tag{12}$$

for all $\beta\in S_j$, $j=0,1$ where

$$(\mathscr{F}_j u)(\alpha) \equiv \int_{-H}^{-\sigma_1} u(z)\varphi^{(j)}(z,\alpha)\,dz. \tag{13}$$

Some careful algebra shows that (12) can be written

$$R_j(\beta) = A_j\delta_{\beta,\alpha_j} - 2\mathrm{i}(-1)^j(B_j^{(2)}(\beta)(\mathscr{F}_j u)(\beta) - B_j^{(1)}(\beta)\mathbf{e}_j^{\mathrm{T}}(\beta)\mathbf{Q}_j), \tag{14}$$

for all $\beta\in S_j$, $j=0,1$ where

$$\mathbf{e}_j(\alpha) = \begin{pmatrix} 1 \\ -D_j f^-(\alpha)\end{pmatrix}, \quad \mathbf{Q}_j \equiv \begin{pmatrix} S^{(j)} \\ Q^{(j)}\end{pmatrix} = \begin{pmatrix} D_j\mathscr{L}^+(\partial_x) \\ 1\end{pmatrix}\partial_x\partial_z\phi^{(j)}(0,-\sigma_j), \tag{15}$$

and where we have defined $\mathscr{L}^{\pm}(\partial_x) = (\partial_x^2 - \alpha_y^2) \mp (1-\nu)\alpha_y^2$. In (15), $S^{(j)}$ and $Q^{(j)}$ represent the unknown shear force and the gradient of elevation (respectively) at the edges of the two ice sheets.

We now apply the first condition in (10) to give

$$A_0\varphi^{(0)}(z,\alpha_0) + \sum_{\alpha\in S_0} R_0(\alpha)\varphi^{(0)}(z,\alpha) = A_1\varphi^{(1)}(z,\alpha_1) + \sum_{\alpha\in S_1} R_1(\alpha)\varphi^{(1)}(z,\alpha). \tag{16}$$

Substituting in from Eq. (14) (with $\alpha$ replacing $\beta$) for the $R_j(\alpha)$ into the above gives the integral equation

$$(\mathscr{K}u)(z) = f(z) \quad \text{for } z\in(-H,-\sigma_1), \tag{17}$$

where

$$\begin{aligned} (\mathscr{K}u)(z) &= \mathrm{i}\sum_{j=0}^{1}\sum_{\alpha\in S_j} B_j^{(2)}(\alpha)(\mathscr{F}_j u)(\alpha)\times\varphi^{(j)}(z,\alpha) \\ &= \sum_{j=0}^{1}\int_{-H}^{-\sigma_1} G^{(j)}(0,z,z_0)u(z_0)\,dz_0, \end{aligned} \tag{18a}$$

$$f(z) = \sum_{j=0}^{1}\left((-1)^j A_j\varphi^{(j)}(z,\alpha_j) + \mathrm{i}\sum_{\alpha\in S_j} B_j^{(1)}(\alpha)\mathbf{e}_j^{\mathrm{T}}(\alpha)\mathbf{Q}_j\varphi^{(j)}(z,\alpha)\right), \tag{18b}$$

and

$$G^{(j)}(x-x_0,z,z_0) = \mathrm{i}\sum_{\alpha\in S_j} B_j^{(2)}(\alpha)\,\mathrm{e}^{\mathrm{i}\alpha|x-x_0|}\varphi^{(j)}(z,\alpha)\varphi^{(j)}(z_0,\alpha) \tag{19}$$

are, as one might expect, Green's functions for the two regions $x<0$ ($j=0$) and $x>0$ ($j=1$), which are well known to have logarithmic singularities as $(x,z)\to(x_0,z_0)$.

### 2.1. Edge conditions

If $h_0>0$, the forcing function, $f(z)$, in (17) contains four unknown constants—$S^{(j)}$ and the $Q^{(j)}$, $j=0,1$ in the two $\mathbf{Q}_j$ vectors—and we will have four edge conditions to apply.

$f$ also contains the two incident waves; so, if we write

$$f(z) = \mathbf{f}^{\mathrm{T}}(z)\hat{\mathbf{Q}}, \quad \hat{\mathbf{Q}}^{\mathrm{T}} = (A_0, A_1, \mathbf{Q}_0, \mathbf{Q}_1),$$

and solve

$$(\mathscr{K}\mathbf{u})(z) = \mathbf{f}(z),$$

the linearity of $\mathscr{K}$ implies that $u = \mathbf{u}^{\mathrm{T}}\hat{\mathbf{Q}}$ solves (17).

If we now substitute this into (14), we can write

$$R_j(\alpha) = \mathbf{r}_j^{\mathrm{T}}(\alpha)\hat{\mathbf{Q}}, \tag{20a}$$

$$\mathbf{r}_0^{\mathrm{T}}(\alpha) = (\delta_{\alpha,\alpha_0}, 0, 2\mathrm{i}B_0^{(1)}(\alpha)\mathbf{e}_0^{\mathrm{T}}(\alpha), 0, 0) - 2\mathrm{i}B_0^{(2)}(\alpha)(\mathscr{F}_0\mathbf{u}^{\mathrm{T}})(\alpha), \tag{20b}$$

$$\mathbf{r}_1^{\mathrm{T}}(\alpha) = (0, \delta_{\alpha,\alpha_1}, 0, 0, -2\mathrm{i}B_1^{(1)}(\alpha)\mathbf{e}_1^{\mathrm{T}}(\alpha)) + 2\mathrm{i}B_1^{(2)}(\alpha)(\mathscr{F}_1\mathbf{u}^{\mathrm{T}})(\alpha). \tag{20c}$$

Now, applying the edge conditions will always involve two manipulations involving the two $\mathbf{Q}_j$ vectors; in addition, we will have to calculate

$$\begin{aligned}\mathbf{P}_j &= \begin{pmatrix} P^{(j)} \\ M^{(j)} \end{pmatrix} = \begin{pmatrix} 1 \\ D_j\mathscr{L}^-(\partial_x) \end{pmatrix}\partial_z\phi^{(j)}(0, -\sigma_j) \\ &= \sum_{\alpha\in S_j}(A_j\delta_{\alpha,\alpha_j} + R_j(\alpha))\mathbf{e}_j(\alpha)\partial_z\varphi^{(j)}(-\sigma_j, \alpha).\end{aligned} \tag{21}$$

$P^{(j)}$ and $M^{(j)}$ represent the displacement and bending moment at the edge of the $j$th sheet.

By (20a), these quantities will depend on $\hat{\mathbf{Q}}$, and by manipulating these as well we eventually obtain four equations in the four unknowns, which we will then solve in terms of the amplitudes of the given incident wave forcings $A_0$ and $A_1$. Potentially then, we need to solve a $4 \times 4$ system, but for the edge conditions that we use this always reduces down to a $2 \times 2$ one, which we write

$$\mathbf{M}_{\mathrm{edge}}\mathbf{Q} = \mathbf{B}\begin{pmatrix} A_0 \\ A_1 \end{pmatrix}, \tag{22}$$

where $\mathbf{Q}$ is an unknown 2-vector.

When $h_0 = 0$, this system actually becomes two scalar equations (see Section 2.1.2 below). There are two main sets of edge conditions that we use, the frozen edge and free edge conditions, which we now introduce.

### 2.1.1. Frozen edge conditions

If the two sheets of ice are frozen together we require that the displacement, the slope of the displacement, the bending moment and the transverse edge force are continuous across the edge. This can be represented by the following equations:

$$\mathbf{Q}_0 = \mathbf{Q}_1, \quad \mathbf{P}_0 = \mathbf{P}_1. \tag{23a,b}$$

Two unknowns (either $\mathbf{Q}_0$ or $\mathbf{Q}_1$) may be eliminated immediately by applying (23a), and the other two may be found by applying (23b). This is done by substituting $u$, the solution to (17) which will depend on the two unknowns, into (14), calculating $P^{(j)}$ and $M^{(j)}$ and using (23b) to create a $2 \times 2$ system of linear equations.

### 2.1.2. Free edge conditions

If the two sheets of ice are free to move independently we require that the bending moments and transverse edge forces must vanish from both sides of the crack.

This can be represented by the following equations:

$$S^{(j)} = 0, \quad M^{(j)} = 0, \tag{24a,b}$$

for $j = 0, 1$. Again we may eliminate two unknowns from the $\mathbf{Q}_j$ vectors using (24a), and we find the remaining two by applying (24b). As with the free edge case, this will usually result in a $2 \times 2$ system of linear equations.

The exception is that if $h_0 = 0$ (i.e. if the left hand region is open water without an ice cover) then the forcing term corresponding to that side,

$$\mathrm{i}\sum_{\alpha\in S_0} B_0^{(1)}(\alpha)\mathbf{e}_0^{\mathrm{T}}(\alpha)\mathbf{Q}_0\varphi^{(0)}(z, \alpha),$$

will vanish as

$$\mathbf{e}_0^{\mathrm{T}}(\alpha)\mathbf{Q}_0 = (1\ \ 0)\begin{pmatrix} 0 \\ Q^{(0)} \end{pmatrix} = 0$$

for all $\alpha \in S_0$. The bending moment $M^{(0)}$ will be zero automatically also, so to find the remaining unknown $Q^{(1)}$ the only condition that we need to apply is $M^{(1)} = 0$.

## 3. Numerical procedure

The solution of the integral equation (17) is approximated using a Galerkin scheme in which, first, the unknown function representing the horizontal component of fluid velocity along $x = 0$ below the corner of the step in a series of even Gegenbauer polynomials. Thus we write

$$u(z) = \frac{2}{H_1}\sum_{n=0}^{\infty} u_n \mathscr{C}_{2n}\left(\frac{z+H}{H_1}\right), \tag{25}$$

where

$$\mathscr{C}_n(t) = \frac{n!(n+\beta)\Gamma^2(\beta)}{\pi 2^{1-2\beta}\Gamma(n+2\beta)}(1-t^2)^{\beta-1/2}C_m^{(\beta)}(t), \tag{26}$$

and $C_m^{(\beta)}(t)$ is a Gegenbauer polynomial. The weighting in the definition above is chosen so that the orthogonality relation

$$2\int_0^1 \mathscr{C}_{2m}(t)C_{2n}^{(\beta)}(t)\,dt = \delta_{mn} \tag{27}$$

is satisfied.

The constant $\beta$ which appears in $u(z)$ allows us to incorporate the required singularity into the fluid velocity at the corner of the ice sheet. In general, at a corner where a fluid region is (locally) contained in wedge of angle $\theta$, the fluid velocity is of the order $r^{\pi/\theta-1}$, where $r$ is the distance to the corner. Specifically, if $H_1 \neq H_2$ then at the bottom left hand corner of the thicker ice sheet $\theta = 3\pi/2$, so $\beta = -\frac{1}{3}+\frac{1}{2} = \frac{1}{6}$ captures the order of the singularity. On the other hand if $H_1 = H_2$ then $\theta = \pi$ and $\beta = 0+\frac{1}{2} = \frac{1}{2}$ is chosen—in this case there is no singularity and we use the Legendre polynomials $P_n(t) = C_n^{1/2}(t)$. Also note that there is never a singularity at the bottom right corner of the thinner ice sheet where the angle is $\theta = \pi/2$ ($\beta = 1$).

The Galerkin scheme involves inserting the series representation (25) into the integral equation (17), multiplying the resulting equation by $\mathscr{C}_{2m}((z+H)/H_1)$ and integrating over $-H < z < \sigma_1$. This procedure results in the infinite linear system of algebraic equations

$$\sum_{j=0}^{1}\sum_{n=0}^{\infty} G_{mn}^{(j)}u_n = f_m, \quad m = 0, 1, \ldots, \tag{28}$$

for the coefficients $u_n$. In (28),

$$\begin{aligned} f_m &= 2\int_0^1 \mathscr{C}_{2m}(t)f(H_1t - H)\,dt \\ &= \sum_{j=0}^{1}\left((-1)^j A_j F_m^{(j)}(\alpha_j) + \mathrm{i}\sum_{\alpha\in S_j} B_j^{(1)}(\alpha)\mathbf{e}_j^{\mathrm{T}}(\alpha)\mathbf{Q}_j F_m^{(j)}(\alpha)\right) \end{aligned} \tag{29}$$

and

$$\begin{aligned} G_{mn}^{(j)} &= 4\int_0^1\int_0^1 \mathscr{C}_{2m}(t)G^{(j)}(0, H_1t - H, H_1t_0 - H)\mathscr{C}_{2n}(t_0)\,dt_0\,dt \\ &= \mathrm{i}\sum_{\alpha\in S_j} B_j^{(2)}(\alpha)F_m^{(j)}(\alpha)F_n^{(j)}(\alpha). \end{aligned} \tag{30}$$

In (29) and (30) we have defined

$$F_n^{(j)}(\alpha) = \frac{2}{H_1}\int_{-H}^{-\sigma_1} \varphi^{(j)}(z,\alpha)\mathscr{C}_{2n}\left(\frac{z+H}{H_1}\right)dz$$
$$= 2\,\mathrm{sech}(\gamma H_j)\int_0^1 \cos(\sigma t)\mathscr{C}_{2n}(t)\,dt$$
$$= \frac{(-1)^n\Gamma(\beta)}{\cosh(\gamma H_j)}\left(\frac{\sigma}{2}\right)^{-\beta}(2n+\beta)J_{2n+\beta}(\sigma), \tag{31}$$

where the abbreviation $\sigma = -\mathrm{i}\gamma H_1$ has been used. These functions are defined so that

$$(\mathscr{F}_j u)(\alpha) = \sum_{n=0}^{\infty} u_n F_n^{(j)}(\alpha),$$

and their final expressions come from the result

$$\cos(\sigma t) = \Gamma(\beta)\left(\frac{\sigma}{2}\right)^{-\beta}\sum_{n=0}^{\infty}(2n+\beta)(-1)^n J_{2n+\beta}(\sigma)C_{2n}^{(\beta)}(t), \tag{32}$$

for $-1\leqslant t\leqslant 1$ (Abramowitz and Stegun, 1965, equation 9.1.81).

For the purposes of computation, the infinite system of equations in (28) above is truncated typically to a modest size of order 10.

## 4. The extension to multiple edges

Thus far we have considered the scattering of waves by a single junction in the ice sheet, between two ice sheets of generally different thicknesses and submergence with either frozen or free edges. We wish to consider the interaction of waves with more than one such junction. This is often achieved using a so-called wide spacing approximation (Evans, 1990; Martin, 2006) in which only propagating wave effects are considered in the interaction between two junctions.

Here we have chosen to consider the full unapproximated interaction between junctions within a framework under which the classic wide-spacing results may eventually be recovered as an approximation. Other authors who have used similar ideas are Guazelli et al. (1992) and Porter and Porter (2003).

This involves formulating the interaction at each junction in terms of reflection and transmission matrices (rather than coefficients) which identify the outgoing wave amplitudes in mode $\alpha$ towards $x=\pm\infty$ (i.e. $j=0,1$) due to an incident wave of mode $\beta$ from either $\pm\infty$.

Thus we replace (4) by

$$\phi^{(j)}(x,z) = \sum_{\alpha\in S_j}(A_j(\alpha)\,\mathrm{e}^{\mathrm{i}\alpha x} + R_j(\alpha)\,\mathrm{e}^{-\mathrm{i}\alpha x})\varphi^{(j)}(z,\alpha), \tag{33}$$

the key difference here being the sum over the whole set $S_j$ in the incident wave amplitudes $A_j(\alpha)$ $(j=0,1)$. Then it is not difficult to show that

$$R_0(\alpha) = \sum_{\beta\in S_0} R^+(\alpha,\beta)A_0(\beta) + \sum_{\beta\in S_1} T^-(\alpha,\beta)A_1(\beta), \tag{34a}$$
$$R_1(\alpha) = \sum_{\beta\in S_1} R^-(\alpha,\beta)A_1(\beta) + \sum_{\beta\in S_0} T^+(\alpha,\beta)A_0(\beta), \tag{34b}$$

gives the outgoing wave amplitudes towards $x=\pm\infty$. Thus $R^+(\alpha,\beta)$ represents the waves reflected back from the junction at $x=0$ in mode $\alpha$ from a wave incident from $-\infty$ in mode $\beta$. The matrix element $T^+(\alpha,\beta)$ gives the corresponding wave amplitude transmitted to $x=+\infty$.

It is not difficult to adapt the theory presented in Section 2 to calculate these matrix elements.

In matrix/vector form, (34) can be written, where each element corresponds to the discrete values of $\alpha$ and $\beta$,

$$\mathbf{R}_0 = \mathbf{R}^+\mathbf{A}_0 + \mathbf{T}^-\mathbf{A}_1, \quad \mathbf{R}_1 = \mathbf{R}^-\mathbf{A}_1 + \mathbf{T}^+\mathbf{A}_0. \tag{35a,b}$$

Now suppose we have two junctions in the ice sheet, the first located at $x=0$ and a second at $x=l$. There are now three generally different regions $x<0$, $0<x<l$ and $x>l$ corresponding to $j=0,1,2$ each having their own separation

solutions. Thus we write the potential as

$$\phi(x,z)=\begin{cases}\sum\limits_{\alpha\in S_0}(A_0(\alpha)\,\mathrm{e}^{\mathrm{i}\alpha x}+R_0(\alpha)\,\mathrm{e}^{-\mathrm{i}\alpha x})\varphi^{(0)}(z,\alpha) & \text{for } x\in(-\infty,0),\\ \sum\limits_{\alpha\in S_1}(B_0(\alpha)\,\mathrm{e}^{\mathrm{i}\alpha x}+B_1(\alpha)\,\mathrm{e}^{\mathrm{i}\alpha(l-x)})\varphi^{(1)}(z,\alpha) & \text{for } x\in(0,l),\\ \sum\limits_{\alpha\in S_2}(A_1(\alpha)\,\mathrm{e}^{\mathrm{i}\alpha(l-x)}+R_1(\alpha)\,\mathrm{e}^{\mathrm{i}\alpha(x-l)})\varphi^{(2)}(z,\alpha) & \text{for } x\in(l,\infty).\end{cases}\tag{36}$$

Each junction will then have an associated set of scattering matrices $R_j^{\pm}(\alpha,\beta)$ and $T_j^{\pm}(\alpha,\beta)$, $j=0$ corresponding to $x=0$, the interface between regions 0 and 1 and $j=1$ corresponding to the interface at $x=l$ between regions 1 and 2.

It follows from (35) then that

$$\mathbf{R}_0=\mathbf{R}_0^{+}\mathbf{A}_0+\mathbf{T}_0^{-}\mathbf{D}\mathbf{B}_1,\quad \mathbf{B}_0=\mathbf{T}_0^{+}\mathbf{A}_0+\mathbf{R}_0^{-}\mathbf{D}\mathbf{B}_1,\tag{37,38}$$

$$\mathbf{B}_1=\mathbf{T}_0^{-}\mathbf{A}_1+\mathbf{R}_1^{+}\mathbf{D}\mathbf{B}_0,\quad \mathbf{R}_1=\mathbf{R}_1^{-}\mathbf{A}_1+\mathbf{T}_1^{+}\mathbf{D}\mathbf{B}_0,\tag{39,40}$$

where

$$\mathbf{D}=\mathrm{diag}\{\mathrm{e}^{\mathrm{i}\alpha l}\}|_{\alpha\in S_1}$$

contains either a phase shift or exponential decay as the generated waves travel from one edge to the other. Hence

$$\mathbf{B}_0=(\mathbf{I}-\mathbf{R}_0^{-}\mathbf{D}\mathbf{R}_1^{+}\mathbf{D})^{-1}(\mathbf{T}_0^{+}\mathbf{A}_0+\mathbf{R}_0^{-}\mathbf{D}\mathbf{T}_0^{-}\mathbf{A}_1)\equiv\mathbf{M}_0\mathbf{A}_0+\mathbf{M}_1\mathbf{A}_1,\tag{41}$$

and so (35) holds in this case also, where the scattering matrices for the combined system of two junctions are now given in terms of the individual scattering matrices as

$$\mathbf{R}^{+}=\mathbf{R}_0^{+}+\mathbf{T}_0^{-}\mathbf{D}\mathbf{R}_0^{+}\mathbf{M}_0,\quad \mathbf{R}^{-}=\mathbf{R}_1^{-}+\mathbf{T}_1^{+}\mathbf{D}\mathbf{M}_1,\tag{42a,b}$$

$$\mathbf{T}^{+}=\mathbf{T}_1^{+}\mathbf{D}\mathbf{M}_0,\quad \mathbf{T}^{-}=\mathbf{T}_0^{-}\mathbf{D}(\mathbf{T}_0^{-}+\mathbf{R}_0^{+}\mathbf{D}\mathbf{M}_1).\tag{42c,d}$$

The process described above can then be used iteratively for more than two junctions. Note that computationally, only a small number of evanescent waves are included in the interactions and so each scattering matrix is small. If evanescent effects are completely ignored, the scattering matrices are $2\times 2$ and we return to the familiar case of wide-spacing.

## 5. Edge waves

Evans and Porter (2003) showed that for two identical ice sheets separated by a crack (where $h_0=h_1$ and the free edge conditions are applied at the junction between the two sheets) there are certain wavenumbers $\beta_y$, slightly above the wavenumber $\gamma_0$, at which edge waves may exist and travel along a crack, even in the absence of an incident wave. (They decay exponentially in the direction perpendicular to the crack.) Mathematically, this is equivalent to setting $A_0=A_1=0$, which would then imply that (22) becomes

$$\mathbf{M}_{\mathrm{edge}}\mathbf{Q}=\mathbf{0}.\tag{43}$$

We then allow $\alpha_y$ to be greater than $\gamma_0>\gamma_1$ and by varying it look for non-trivial solutions to (43)—i.e., we find a value of $\alpha_y$ ($\beta_y$) such that the determinant of $\mathbf{M}_{\mathrm{edge}}$ vanishes. The null space of $\mathbf{M}_{\mathrm{edge}}$ then determines the shape of the edge wave (i.e. the value of $\mathbf{Q}$).

By following the same procedure we will investigate whether or not these edge waves may also exist when $h_0\neq h_1$.

## 6. Results

We begin this section by presenting some initial results which illustrate the range of geometries and combinations of edge conditions that can be treated with this method. These results are verified using independent methods wherever possible.

Particular attention is paid to the problem of scattering by leads, and to the convergence of the wide-spacing approximation (WSA) for leads. (A lead is a region of open water or thin ice enclosed between two different ice sheets, and we deal with it by the multiple-scattering method of Section 4.) We concentrate on leads so much primarily because

Williams and Squire (2008b) showed that the scattering of large ice fields is dominated by the scattering of the leads contained in them (in comparison to other irregularities such as pressure ridges).

We finish the section by extending the investigation of Evans and Porter (2003) into the existence of edge waves along a crack between two ice sheets. They observed them numerically when the ice sheets on either side of the crack had identical thicknesses, and we investigate how long they persist when one or other of the thickness is changed. It is found that only a tiny change is needed to completely obliterate them.

### 6.1. Sample results and verification

Let us define a reflection coefficient $\mathscr{R} = R^+(\alpha_0, \alpha_0)$. The quantity that we are most interested in is its magnitude, $|\mathscr{R}| = |R^+(\alpha_0, \alpha_0)| = |R^-(\alpha_1, \alpha_1)|$, which is the amplitude of the reflected wave if a unit amplitude wave propagating wave arrives at the feature in question *either* from the left *or* from the right. Our first check is that it and the transmission coefficient $\mathscr{T} = T^+(\alpha_1, \alpha_0)$ satisfy the energy conservation relationship $|\mathscr{R}|^2 + s|\mathscr{T}|^2 = 1$, where $s = B_0^{(2)}(\alpha_0)/B_1^{(2)}(\alpha_1)$ is called the intrinsic admittance. This relationship is satisfied to machine precision, as is typical for variational methods such as the Galerkin method Porter (1995).

Now, there are many different ways of calculating the scattering by edges between ice sheets when the effects of submergence are neglected, and so we continue our verification by testing that our method works in that case. Recall that this is simply a matter of using the $C_n^{(1/2)}$ polynomials (also known as the Legendre polynomials) instead of the $C_n^{(1/6)}$ polynomials. Fig. 2(a) shows the amount of reflection by a single edge when $h_1 = 1\,\mathrm{m}$, $H_1 = 20\,\mathrm{m}$ and $h_0 = 0$ (solid line), 0.5 m with free edge conditions (dashed line) and 0.5 m with frozen edge conditions (dotted line). The dots

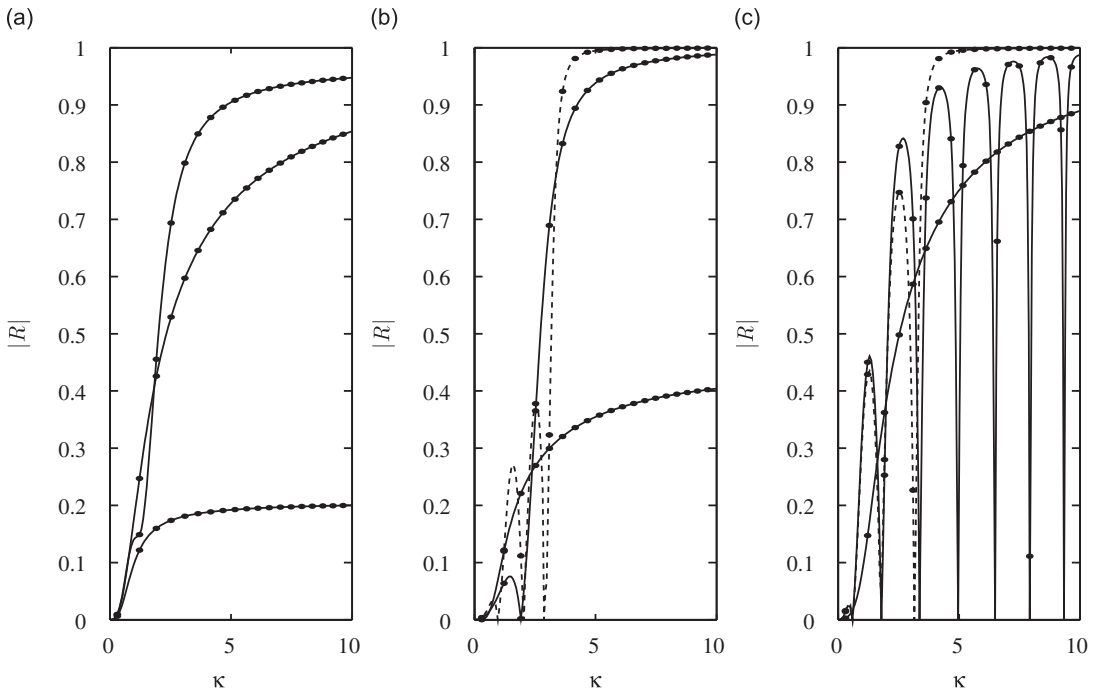


Fig. 2. Sample results when the effect of submergence is neglected. (a) The solid line shows the scattering by a single edge when $h_0 = 0$, while the dashed and dotted lines show the scattering when $h_0 = 0.5\,\mathrm{m}$ and when either the free edge or frozen edge conditions are applied (respectively). For all cases $h_1 = 1$ and $H_1 = 20\,\mathrm{m}$. (b) The solid line shows the scattering by a pair of edges when $h_0 = h_2 = 0$, while the dashed and dotted lines show the scattering when $h_0 = h_2 = 0.5\,\mathrm{m}$ and when either the free edge or frozen edge conditions are applied (respectively, and at both edges). For all cases the waves are normally incident, $h_1 = 1$, $H_1 = 20$ and $l = 15\,\mathrm{m}$ (only applicable in (b) and (c)). (c) The solid line shows the scattering when $h_0 = h_2 = 1$, $H_0 = 20\,\mathrm{m}$, $h_1 = 0$, while the dashed line shows the scattering when $h_1 = 0.5\,\mathrm{m}$ and the free edge conditions are applied (at both edges). The dotted line shows the scattering when $h_0 = 0$, $h_1 = 1$, $h_2 = 0.5$ and $H_1 = 20\,\mathrm{m}$. The frozen edge conditions are applied at the joint between the two ice sheets, and $l = 15\,\mathrm{m}$. *Checks*: The dots in (a) compare our results with those from a different eigenfunction matching method (Evans and Porter, 2003), while the dots in (b) and (c) compare our results with those from that same eigenfunction matching method when they are extended using (42).

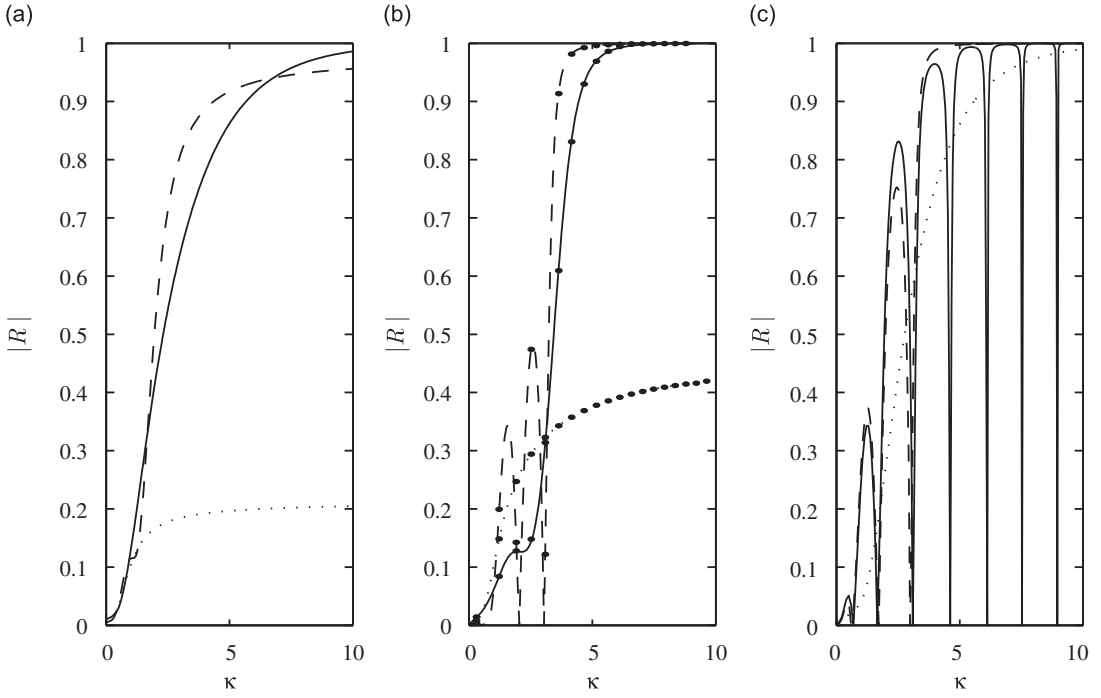


Fig. 3. Sample results when the effect of submergence is included. The curves shown in all the figures correspond to the same geometries used in Fig. 2. *Checks*: The dots plotted in (b) compare the results using the method of Williams and Squire (2008a), who used Green's theorem.

that fall on each line are the result of doing the same calculations but with the eigenfunction matching method (EMM) as it is usually used (Sahoo et al., 2001; Evans and Porter, 2003) instead of coupling it to a Galerkin scheme as we do—as can be seen the two different methods give very good agreement. The curves are all plotted against $\kappa = (L\omega^2)/g$, the non-dimensional open water, infinite depth wavenumber.

In Fig. 2(b), we add the mirror image of the edge in Fig. 2(a), 15 m to the right of that edge, so that the solid line represents a 15-m-wide, 1-m-thick floe in open water, and the other lines represent the same floe embedded in a 0.5-m-thick ice sheet, with the free (dashed) and frozen (dotted) edge conditions applied at both edges.

Fig. 2(c) is similar to Fig. 2(b): the solid and dashed lines represent 15-m-wide leads in a 1-m-thick ice sheet, the former showing the reflection when the lead just contains open water while the latter contains 0.5-m-thick ice with free edges. For a little variation, however, the dotted line shows the scattering by a 15-m-wide, 1-m-thick floe with open water on the left and 0.5-m-thick ice on the right. Frozen edge conditions are applied at the edge between the floe and the ice sheet.

In both Figs. 2(b) and (c), the dots plotted are calculated with the usual EMM combined with our the multiple edge result (42) and show excellent agreement with our results.

Fig. 3 shows reflection results for the same geometries as in Fig. 2, but when the effects of submergence are included. The results in (b) were checked using the method of Williams and Squire (2008a) who used Green's theorem and good agreement was obtained, as can be seen by the dots plotted. Unfortunately, no independent methods were available to us for checking the results of either (a) or (c) as Green's theorem method does not work for semi-infinite regions, for when the two outer thicknesses are different, or when the middle thickness is smaller than the outer ones. However, as the results of (a) are needed to obtain those in (b), we are fairly confident in those ones also. In support of those in (c), they are calculated in exactly the same way as those in (b) so we are quite confident of them also. Moreover, all the no-submergence results were confirmed with the EMM method, and as mentioned above "switching" the effects of submergence "on" or "off" only involves the fairly minor change of swapping one set of Gegenbauer polynomials for another.

In terms of the actual scattering patterns shown in Figs. 2(a) and 3(a), including the effects of submergence when both sides of the transition are covered with ice makes little difference. In both figures the reflection curves initially climb steeply as $\kappa$ increases from zero, before leveling off in the short wave limit to about 0.94 and 0.20 when the free and

frozen edge conditions are applied, respectively. In contrast, including submergence when $h_0 = 0$ produces quite marked changes in the reflection predicted—particularly for short waves when $|R| \approx 0.86$ without submergence but increases to about 0.99 with submergence at $\kappa = 10$. There is also slightly more reflection as $\kappa \to 0$ when submergence is included—the limiting value is predicted by Lamb (1932) to be $(1 - \sqrt{H_1/H_0})/(1 + \sqrt{H_1/H_0})$. However, including submergence produces less scattering for $\kappa$ in the interval $(.42, 2.28)$ (for periods between 4.6 and 13 s) than is predicted without submergence.

Moving to Figs. 2(b) and 3(b), it can be seen that submergence now produces slightly more reflection when the central ice strip is frozen than when submergence is neglected. Similarly, when the floe's edges are free the two peaks in reflection at $\kappa \approx 1.6$ and $\kappa \approx 2.6$ are about 0.05 and 0.10 greater when submergence is included than when it isn't. For the floe in open water, apart from the relative sizes of $|R|$ which are basically the same as in Figs. 2(a) and 3(a), the main difference between the two cases is the zero in reflection that appears in Fig. 2(b) but which becomes a minimum in Fig. 3(b). Williams and Squire (2008a) showed that when heave is included as well as submergence the zero reappears.

The most noticeable aspect of Figs. 2(c) and 3(c) are the large number of maxima and minima in the open lead graphs. These are due to resonances between the lead edges and the wavelength for open water. The wavelength for ice is much longer which is why fewer resonances are seen when the lead is filled with ice. No resonances are expected for when the two outer regions are different.

Again, comparing Fig. 2(c) to Fig. 3(c) submergence seems to have more effect when open water is present. The scattering by the ice-filled lead is essentially the same whether or not submergence is considered, while in the other two cases submergence produces noticeably more reflection at low and high $\kappa$, but less reflection for an intermediate range.

Figs. 4 and 5 both show the dependence of the scattering by different edges on the angle of incidence. The periods used in both are 11.8 s (solid lines, $\kappa = 0.5$), 7.67 s (dashed lines, $\kappa = 1$), and 4.97 s (dotted lines, $\kappa = 2$). As in Fig. 3(b), results in Figs. 4(b) and 5(b) are both checked against Green's function method of Williams and Squire (2008a), with very good agreement being found (as can be seen from the dots plotted on the figures).

The most obvious feature of Figs. 4(a) and 5(a) is the existence of a critical angle beyond which there is complete reflection. These follow from the relation $\alpha_y = \gamma_0 \sin\theta_0 = \gamma_1 \sin\theta_1$; if $\gamma_1 < \alpha_y < \gamma_0$ then no propagating waves are able to travel into the right hand region. In addition, they are higher when the left hand region is covered with ice than when it is just open water. This is because the two wavenumbers are closer when both regions have an ice cover—increasing $h_0$ up to $h_1$ makes $\gamma_0$ drop to $\gamma_1$ (wavelength increases with ice thickness).

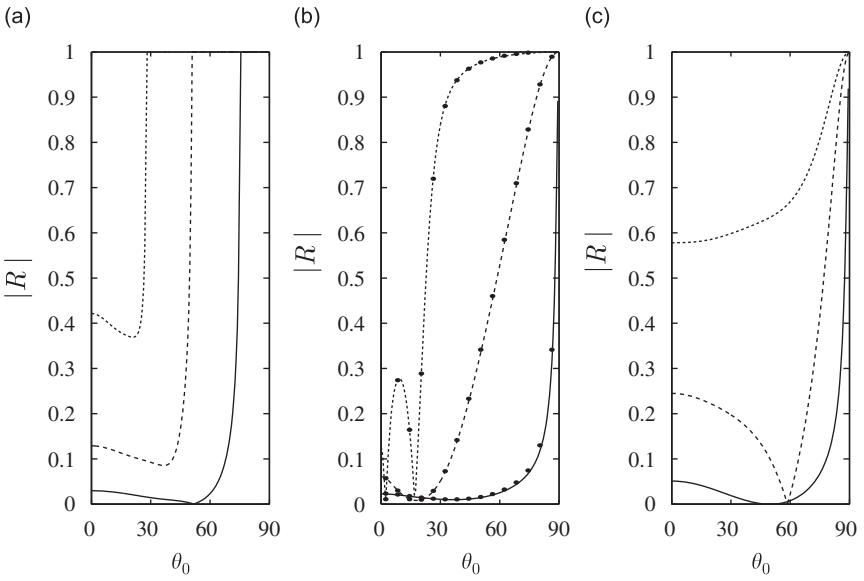


Fig. 4. The dependence of the scattering by edges between open water regions and regions of 1-m-thick ice on the angle of incidence. The geometries in (a), (b) and (c) are the same as for the solid lines in Figs. 3(a), (b) and (c), respectively. The different lines correspond to $\kappa = 0.5$ (solid, wave period is 11.8 s), $\kappa = 1$ (dashed, wave period is 7.67 s) and $\kappa = 2$ (dotted, wave period is 4.97 s), and the waves arrive from the left hand region. $\min\{H_j \,|\, j = 0, 1, 2\} = 20$ m and submergence effects are included. *Checks*: The dots plotted in (b) compare the results using the method of Williams and Squire (2008a), who used Green's theorem.

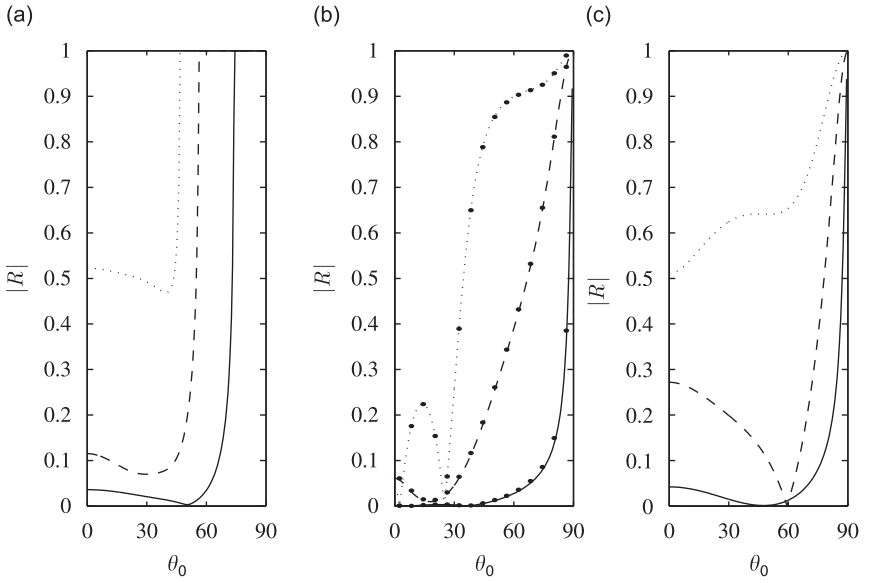


Fig. 5. The dependence of the scattering by free edges between regions of 0.5-m-thick and 1-m-thick ice on the angle of incidence. The geometries in (a), (b) and (c) are the same as for the dashed lines in Figs. 3(a), (b) and (c), respectively. The different lines correspond to $\kappa = 0.5$ (solid), $\kappa = 1$ (dashed) and $\kappa = 2$ (dotted) and the waves arrive from the left hand region. $\min\{H_j \,|\, j = 0, 1, 2\} = 20\,\text{m}$ and submergence effects are included. *Checks*: The dots plotted in (b) compare the results using the method of Williams and Squire (2008a), who used Green's theorem.

For smaller angles of incidence, the behaviour is very simple—as it increases it from normal incidence, $|R|$ drops slightly to a minimum or a zero before climbing to 1 at the critical angle. And as expected, smaller periods produce more reflection—which is also true in general for Figs. 4(b, c) and 5(b, c).

The addition of an extra edge in Figs. 4(b) and 5(b) adds somewhat more fine structure to the lower period curves, particularly when a floe is floating in open water (Fig. 4b) or when it is embedded in thinner ice (Fig. 5b). In both $\kappa = 2$ curves, a pair of zeros can be seen and when $h + 0 = 0.5\,\text{m}$ an inflexion point is apparent. In general, though the behaviour is fairly simple—$|R|$ increases to 1 as the angle of incidence is increased up to 90°. We might have expected there to have also been a critical angle apparent in this case—the fact there isn't is due to the extra interactions waves between the two edges due to evanescent waves. That these are able to have an effect is due to the relatively short floe width (15 m); at the smallest period, when $l$ would be the largest compared to the wavelength in the floe we see very large but not quite total reflection when $h_0 = 0$. If $l$ were increased enough for the evanescent waves to die down before they reach the edge, we would expect to see the critical angle behaviour re-appearing.

In Figs. 4(c) and 5(c), it is the higher period curves that have the more structure. Both pairs of $\kappa = 0.5$ and 1 curves drop to single zeros before climbing to 1 in the grazing-incidence limit. The $\kappa = 2$ curve in Fig. 4(c) simply climbs monotonically to 1, although its counterpart in Fig. 5(c) contains a slight inflexion.

The final figure in this section, Fig. 6, reproduces the results for the leads in Figs. 2(c) and 3(c), but this time compares the exact results with the WSA (Evans, 1990; Martin, 2006). The solid curves, which represent exactly the scattering by open leads without (a) and with (b) submergence included, are compared to WSA results which are plotted as dots. Other authors [e.g. Vaughan et al. (2007)] have already established this result when submergence is not considered, but we wished to demonstrate that the WSA result for an open lead is also very accurate when it is considered. This result is very important for calculating the scattering by multiple leads as using the WSA greatly accelerates such computations.

### 6.2. Edge waves

Fig. 7 shows an example of what the displacement profile of an edge wave along a crack of period 7.67 s (chosen to make $\kappa = 1$) in a 1-m-thick ice sheet looks like. The wave profile is sinusoidal in the direction parallel to the crack, but it has a very slow exponential decay as you travel away from the crack. $\beta_y/\gamma_0 = 1.0002$, making its wavelength 118.79 m, only 0.02% smaller than the usual wavelength for a wave of this period under a 1-m-thick ice sheet (118.82 m).

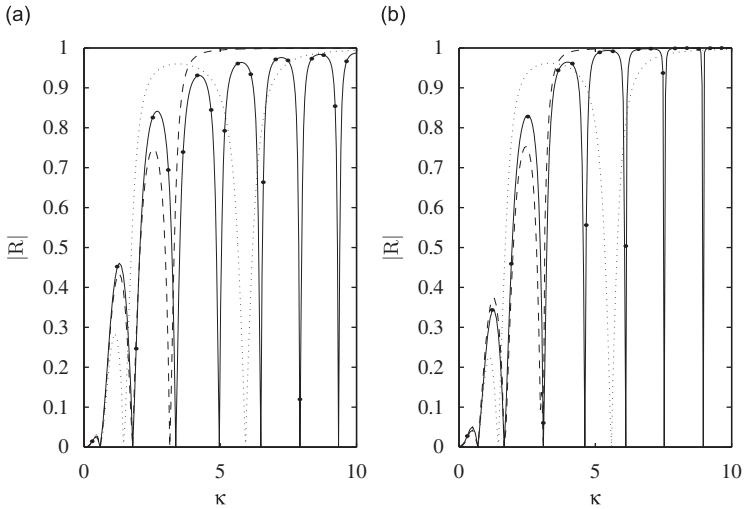


Fig. 6. Verification of the accuracy of the wide-spacing approximation for leads. In all situations the waves are normally incident, $h_0 = h_2 = 1\,\text{m}$, $H_0 = 20\,\text{m}$, and $l = 15\,\text{m}$, and the results in (a) do not include the effects of submergence while the results in (b) do. Solid lines show the (exact) scattering when $h_1 = 0$, while the dots show the wide-spacing results for comparison. Dashed lines show the (exact) scattering when $h_1 = 0.5\,\text{m}$ and the free edge conditions are applied at both edges, while the dotted lines show the wide-spacing results for comparison.

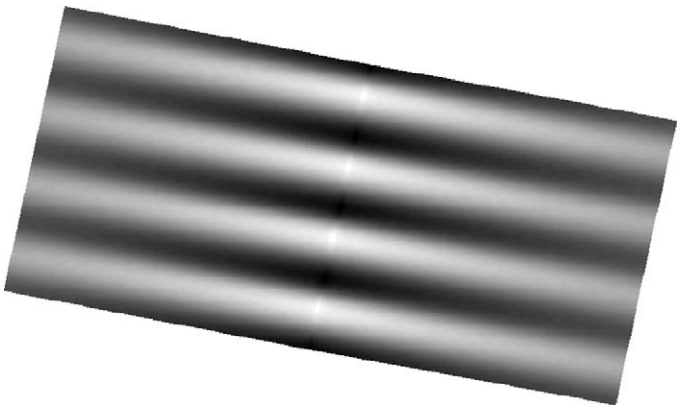

Fig. 7. Displacement profile as an edge wave travels along a crack when $h_0 = h_1 = 1\,\text{m}$, period $= 7.67\,\text{s}$ ($\kappa = 1$) and $H_1 = 20\,\text{m}$. $\beta_y/\gamma_0 = 1.0002$, making its wavelength 118.79 m (compared to 118.82 m, which is the usual wavelength for a wave of this period in water of this depth under a 1-m-thick ice sheet). Note the gradual decay of the wave with distance from the crack.

Fig. 8 shows that the wavelength of any edgewave along a crack is extremely close to the usual ice wavelength for all periods, although it is slightly more different for small periods. The figure plots $\beta_y/\gamma_0 - 1$, the difference between the two wavenumbers as a fraction of $\gamma_0$ itself, against $\kappa$ when $h_0 = h_1 = 1\,\text{m}$, and it appears that the difference is usually no more than 0.06%.

We now investigate what happens to the edge waves when we change the thickness of the left hand ice-sheet slightly, so that the sheets on either side of the crack are no longer identical. Fig. 9 shows that when $\kappa = 1$ and $h_1 = 1\,\text{m}$, either increasing or decreasing $h_0$ from $h_1$ causes $\beta_y$ to decrease towards $\gamma_M = \max\{\gamma_0, \gamma_1\}$. When the two thicknesses differ by about 2 mm, $\beta_y$ becomes equal to $\gamma_M$. In this situation the wave no longer decays exponentially on both sides, but persists to $|x| \to \infty$ in the direction where the ice is thinnest. Defining some parameters $\delta_\pm$ such that the two times that $\beta_y = \gamma_M$ occur when $h_0/h_1 = 1 + \delta_\pm$, we can now say that unless $\delta_- \leqslant h_0/h_1 - 1 \leqslant \delta_+$, no edge waves can exist.

Fig. 10 plots $\delta_\pm$ for a range of $\kappa$ when $h_0 = 1\,\text{m}$. It shows that for these $\kappa$ if $h_0$ is less than about 5 mm different from this $h_1$, then no edge waves can exist. In addition, as the wavelengths increase, the interval in which edge waves can exist

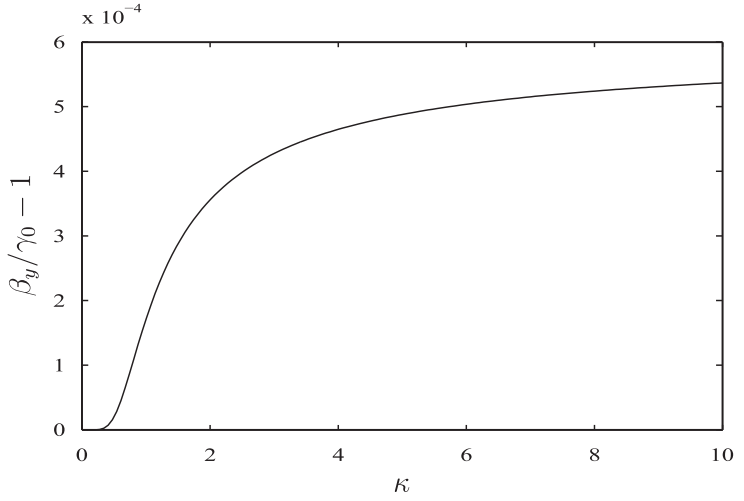


Fig. 8. Dependence of the edge-wave wavenumber $\beta_y$ on $\kappa$ when $h_0 = h_1 = 1\,\mathrm{m}$ and $H_1 = 20\,\mathrm{m}$.

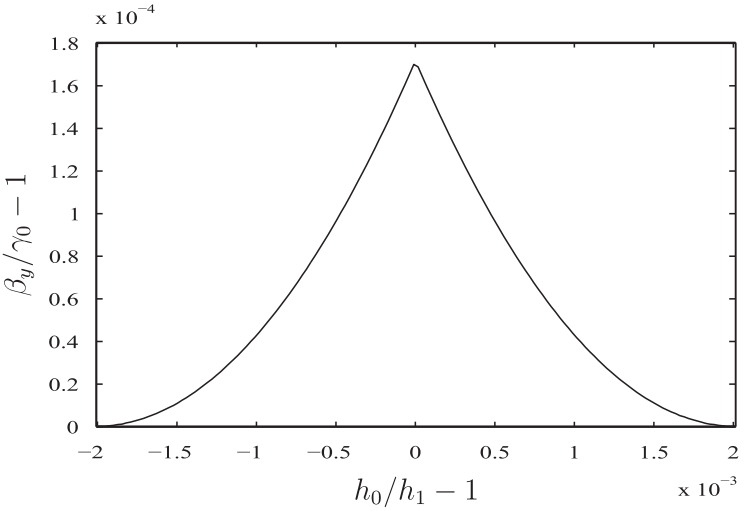


Fig. 9. Dependence of the edge-wave wavenumber $\beta_y$ on $h_0$ when $h_1 = 1\,\mathrm{m}$, period $= 7.67\,\mathrm{s}$ ($\kappa = 1$) and $H_1 = 20\,\mathrm{m}$.

shrinks to zero, and the largest intervals occur for smaller wavelengths. Such small tolerances suggest that edge waves are unlikely to ever exist along a real crack between two semi-infinite ice sheets, as the ice on either side would essentially have to be exactly the same.

## 7. Conclusions

In this paper, we have formulated the solution to a canonical problem of the scattering of an incident flexural-gravity wave by an interface between two ice sheets of differing properties in terms of a scattering matrix formulation which allows the retention of both propagating and evanescent modes when dealing with multiple edges. The formulation used is exact under linearised theory. A particular novel feature of the present paper is that we have allowed variable submergence of the ice sheets in accordance with Archimedes' principle, in contrast the majority of other related work in this research area. Full generality has been assumed in the choice of ice sheet properties so that, for instance, the ice thickness may be reduced to zero yielding an open water free surface. In addition, we have also generalised the connections between two ice sheets to be either frozen or free edges.

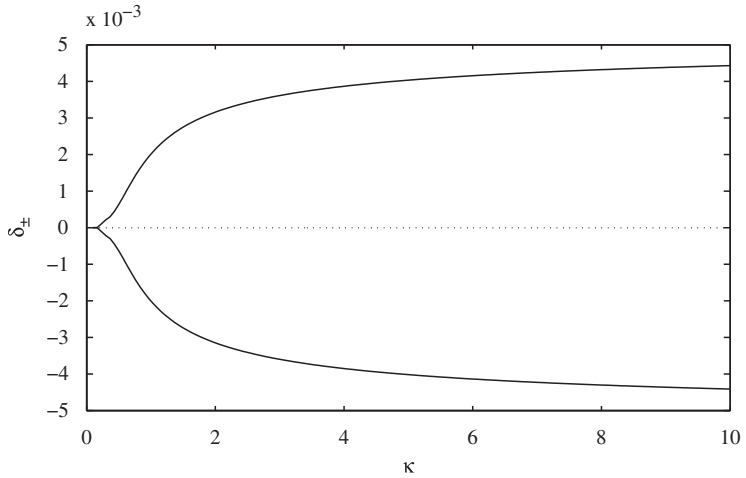


Fig. 10. Range of values for $h_0$ for which edge waves may exist when $h_1 = 1\,\mathrm{m}$ and $H_1 = 20\,\mathrm{m}$. $\delta_-$ is the lower curve, while $\delta_+$ is the upper curve.

We have solved the canonical scattering problem involving a single interface by formulating integral equations for unknown functions related to the horizontal velocity below the interface and solving by a numerically efficient and accurate Galerkin-based scheme. This approach also has the advantage of being able to take corner singularities into account, which also enhances the convergence of our results.

Our formulation has been presented in an extremely general way, to explain how the scattering by multiple edges, and thus by multiple irregularities such as leads and pressure ridges, can be computed.

We have also been able to extend the results of Evans and Porter (2003) and demonstrate the existence of edge waves propagating between two ice sheets of different thicknesses. However, these edge waves do not persist if the thickness of one of the sheets is changed more than slightly.

## References

Abramowitz, M., Stegun, I., 1965. Handbook of Mathematical Functions. Dover Publications, New York.

Bennetts, L.G., Biggs, N.R.T., Porter, D., 2007. A multi-mode approximation to wave scattering by ice sheets of varying thickness. Journal of Fluid Mechanics 579, 413–443.

Evans, D.V., Porter, R., 2003. Wave scattering by narrow cracks in ice sheets floating on water of finite depth. Journal of Fluid Mechanics 484, 143–165.

Evans, D., 1990. The wide-spacing approximation applied to multiple scattering and sloshing problems. Journal of Fluid Mechanics 210, 647–658.

Guazelli, E., Rey, V., Belzons, M., 1992. Higher-order Bragg reflection of gravity surface waves by periodic beds. Journal of Fluid Mechanics 245, 301–317.

Kohout, A., Meylan, M., Sakai, S., Hanai, K., Leman, P., Brossard, D., 2007. Linear water wave propagation through multiple floating elastic plates of variable properties. Journal of Fluids and Structures 23 (4), 649–663.

Lamb, H., 1932. Hydrodynamics. Cambridge University Press, Cambridge.

Linton, C., McIver, P., 2001. Handbook of Mathematical Techniques for Wave/Structure Interactions. CRC Press, Boca Raton, FL.

Martin, P., 2006. Multiple Scattering. Interaction of Time Harmonic Waves with N Obstacles. Cambridge University Press, Cambridge.

Meylan, M., Squire, V., 1994. The response of ice floes to ocean waves. Journal of Geophysical Research 99, 899–900.

Porter, D., Porter, R., 2004. Approximations to wave scattering by an ice sheet of variable thickness over undulating bed topography. Journal of Fluid Mechanics 509, 145–179.

Porter, R., Porter, D., 2003. Scattered and free waves over periodic beds. Journal of Fluid Mechanics 483, 129–163.

Porter, R., 1995. Complementary methods and bounds in linear water waves. Ph.D. Thesis, University of Bristol, Bristol, United Kingdom.

Sahoo, T., Yip, T., Chwang, A., 2001. Scattering of surface waves by a semi-infinite floating elastic plate. Physics of Fluids 13, 3215–3222.

Squire, V., Dixon, T., 2000. An analytical model for wave propagation across a crack in an ice sheet. International Journal of Offshore and Polar Engineering 10, 173–176.

Vaughan, G., Williams, T., Squire, V., 2007. Perfect transmission and asymptotic solutions for reflection of ice-coupled waves by inhomogeneities. Wave Motion 44 (5), 371–384.

Wadhams, P., 1988. Sea ice morphology. In: Lapparanta, M. (Ed.), Physics of Ice Covered Seas, vol. 1. Helsinki University Printing House, NJ, pp. 231–287.

Wang, C., Meylan, M., Porter, R., 2007. The linear wave response of a periodic array of floating elastic plates. Journal of Engineering Mathematics 57 (1), 23–40.

Williams, T.D., Squire, V.A., 2007. Wave scattering at the sea-ice/ice-shelf transition with other applications. SIAM Journal on Applied Mathematics 67 (4), 938–959.

Williams, T.D., Squire, V.A., 2008a. The effect of submergence on scattering across a transition between two floating flexible plates. Wave Motion 45 (3), 361–379.

Williams, T.D., Squire V.A., 2008b. Wave propagation across sea-ice thickness changes. Ocean Modelling 21 (1–2), 1–11.

Williams, T., Squire, V., 2004. Oblique scattering of plane flexural-gravity waves by heterogeneities in sea ice. Proceedings of the Royal Society of London Series A 460, 3469–3497.

Wu, C., Watanabe, E., Utsunomiya, T., 1995. An eigenfunction expansion-matching method for analyzing the wave-induced responses of an elastic floating plate. Applied Ocean Research 17 (5), 301–310.